Research Paper /

Mass Transfer from Mobile to Immobile Regions in Irregularly-Shaped Micro-Channels at Low Reynolds Number

Kizuki Toyama[†]

[†] Division of Sustainable Resources Engineering, Faculty of Engineering, Hokkaido University, N13-W8, Sapporo, Hokkaido, 060-8628, Japan

Fumina Togi[†]

[†] Division of Sustainable Resources Engineering, Faculty of Engineering, Hokkaido University, N13-W8, Sapporo, Hokkaido, 060-8628, Japan

Shusaku Harada[†*]

[*]Corresponding author,
[†] Division of Sustainable Resources Engineering, Faculty of Engineering, Hokkaido University, N13-W8, Sapporo, Hokkaido, 060-8628, Japan, harada@eng.hokudai.ac.jp

Conflict of Interest: None.

Keywords: solute dispersion, micro-channel, MIM model

Article Impact Statement:

The solute dispersion in variously-shaped micro-channels shown here would contribute to the understanding of mass transfer in groundwater.

ABSTRACT

Transient mass transfer in rough-walled micro-channels was investigated experimentally. We conducted experiments using rough-walled channels with various irregularities at small Reynolds number conditions. Mass transfer in the mainstream (mobile region) and dead water region (immobile region) were quantified using an image analysis technique based on absorption photometry. The experimental results showed that the solute dispersion in the mobile region was influenced by the irregular shape of the channel wall complicatedly. In contrast, mass transfer in the immobile region occurred by molecular diffusion independently on the wall roughness in our experimental conditions. The irregular shape of channel wall may enhance the mass transfer in mobile region by distorting the velocity distribution (Togi et al., 2020), while the solute redistribution to immobile region may suppress it in streamwise direction, just on a longer time scale. We developed a mass transfer model analogous to Mobile–Immobile model (MIM model) proposed by previous studies. The concept of the model is the same as the previous study (Zhou et al., 2019) and the coefficients of the model describing mass transfer in each region were quantified from the experimental results as functions of geometric characteristics of the rough-walled channel. In addition, mass transfer coefficient from mobile to immobile regions were derived mathematically based on the experimental results. The MIM model with the coefficients derived in this study well describes solute dispersion in variously-shaped irregular channels quantitatively.

Introduction

Solute dispersion in liquid-filled micro-channels is widely observed in various fields such as pollution transport underground (Domenico and Schwartz, 1998) or reactive flow in micro-channels (Stone et al. 2004). In most cases, the dispersion process in the network of micro-channels, such as soils, rock cracks or porous media, has been studied from a macroscopic perspective with parameters of void characteristics, i.e., void fraction or tortuosity (Jury and Horton, 2004).

Meanwhile, the dispersion behavior in individual micro-channels is complicatedly dependent on their inner shape. Therefore it has been studied from a microscopic perspective. As is well-known, the longitudinal dispersion of solutes in a micro-channel is determined by a combination of the molecular diffusion of solutes and the nonuniform velocity of the solvent in the channels (Taylor, 1953; Aris, 1959). Consequently, the dispersion coefficient in a channel is influenced by geometric conditions of the channel such as size, cross-sectional shape and wall roughness, because they bring about differences in the velocity profile of the solution in the channels. The effect of channel cross-sectional shapes on solute dispersion has been studied (Doshi et al. 1978; Chatwin, 1982; Aris, 1959; Fukushima, 1983; Dutta et al. 2006; Ajdari et al. 2006). These studies found that the cross-sectional shape of the channel dramatically affects the longitudinal dispersion of solutes.

The wall roughness of the channel also influences the solute dispersion. Particularly its effect is apparent under moderate Péclet number conditions (Roux et al. 1998; Detwiler et al. 2000). The wall roughness brings about the variance of flow velocity in the channel. As a result, the dispersion behavior in a rough-walled channel is complicatedly dependent on the geometric conditions as well as the flow conditions (Thompson, 1991; Koplik et al. 1993; Bouquain et al. 2012; Zhou et al. 2019, Wang et al. 2020; Yoon and Kang, 2021). Additionally, the wall roughness plays a wide variety of roles in solute dispersion. The roughness with a small amplitude enhances the longitudinal dispersion in the mainstream by increasing the velocity variance (Roux et al. 1998), whereas the roughness with a large amplitude leads to dead water regions near the wall (Lee et al. 2014; Briggs et al. 2017). Togi et al. (2020) experimentally examined the effect of wall roughness on solute dispersion using

variously-shaped quasi-two-dimensional micro-channels. They established the dispersion model in the channel including the effect of wall roughness as functions of the geometric properties such as the amplitude and the wavelength of the roughness. They also reported that the existence of the dead water region is a key role in solute dispersion in longitudinal direction.

The effect of the dead water region on the solute dispersion has been studied for an extended period. Coats and Smith (1964) established the first concept of the Mobile-Immobile model (MIM model) in which the mass transfer in the channel is considered as the combination of the transfer in the mobile region (mainstream), the transfer in the immobile region (i.e., dead water region, stagnant region or recirculation zone) and the transfer between mobile-immobile regions. Some researchers have developed this concept through mass transfer in porous media (van Genuchten and Wierenga, 1976; Haggerty and Gorelick, 1995; Gao et al. 2010; Porta et al. 2013). Recently, Zhou et al. (2019) conducted numerical simulations on solute transfer in a rough-walled channel under moderate Reynolds number and large Péclet number conditions. They proposed a new mobile-immobile model called the DMIM model (distributed MIM model) for mass transfer in a channel with irregular shape and established differential equations that successfully describe the temporal change of solute concentration in the channel.

In this study, we examined a transient mass transfer in an irregular-shaped channel at low Reynolds number and moderate Péclet number conditions experimentally. Our main purpose is to establish a comprehensive dispersion model that expresses the transient solute dispersion including molecular diffusion, wall roughness and channel cross-sectional shape effect. We developed a dispersion model which contains both the rough-wall effect on longitudinal dispersion in the mobile region (main flow region) by Togi et al. (2020) and the distribution of solutes into the immobile region (dead water region) by Zhou et al. (2019). Our main mission is to relate parameters of the model to geometric properties of the channel and extract the physical essence of mass transfer in an irregular-shaped channel at low Reynolds number conditions. The results of established model were compared to the experimental results of solute concentration profiles in a quasi-two-dimensional

channel. In the experiment, the concentration field of solute was quantified by a method based on adsorption photometry. We evaluated the coefficients in the model as functions of the geometric properties of the channel and flow conditions.

Model concepts

In this study, we focused on the solute dispersion in a liquid-filled micro-channel with complicated geometries. As an example, the left side in Figure 1 indicates a visualized image of the concentration field of cupric ions in a glycerin-filled irregular-shaped channel, which is obtained by Togi et al. (2020). As can be seen, the solute migrates selectively at the center of the channel (green and yellow part), and the dead water regions exist in the vicinity of the channel wall (blue part). The dead water regions narrow the apparent width of the channels. Consequently, the concentration field is distorted and sharpened at the center. This example shows that the wall roughness impacts mass transfer in the streamwise direction.

The right side in Fig.1 specifies the conceptual image of the dispersion model in a rough-walled channel proposed by Zhou et al. (2019). In the model, the channel is separately considered as mobile (mainstream) and immobile regions. This kind of model is known as the Mobile-Immobile model (MIM model) which has been developed to describe mass transfer in complicated void networks like porous media (van Genuchten and Wierenga, 1976; Haggerty and Gorelick, 1995; Gao et al. 2010; Porta et al. 2013). Zhou et al. (2019) performed numerical simulations on mass transfer in an irregular shaped channel at moderate Reynolds number conditions (Re=10~150) and discussed the transfer process in mobile and immobile regions by the MIM model shown in Fig.1. They reported that recirculation flow in the immobile region played a significant role in mass transfer near the wall and established the DMIM (distributed MIM) model describing mass transfer in the channel as follows.

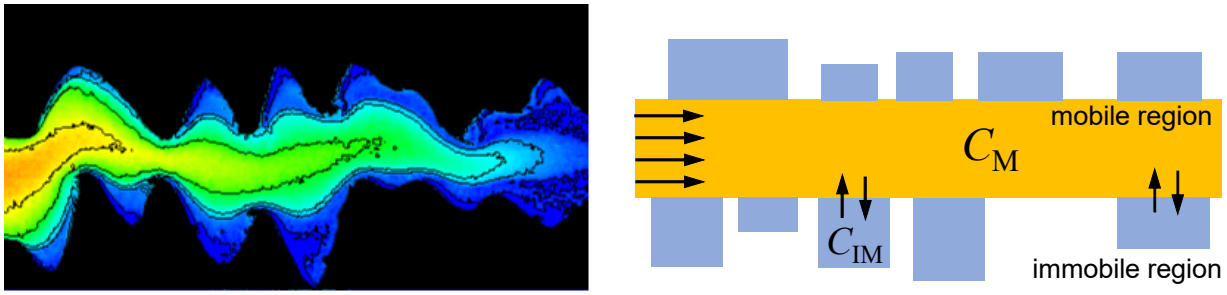

Fig.1 Conceptual image of dispersion model (left: visualized image of concentration field by Togi et al. (2020) (red:high solute concentration, blue low solute concentration); right: concept of DMIM model by Zhou et al. (2019).

$$(1-\theta)\frac{\partial C_M}{\partial t}+\theta\frac{\partial \overline{C_{IM}}}{\partial t}=(1-\theta)D_x\frac{\partial^2 C_M}{\partial x^2}-v\frac{\partial C_M}{\partial x} \tag{1}$$

where $C_M(x, t)$ is the cross-sectional averaged concentration in the mobile region and and $\overline{C_{IM}}(x, t)$ is the averaged concentration in immobile region at position $x=x$, θ is the ratio of the immobile region to total volume at each cross-sectional position, v is advection velocity in the mobile region, and D_x is the longitudinal dispersion coefficient in the mobile region. Mass transfer between mobile and immobile regions at the position of each immobile region x is expressed as follows.

$$\frac{\partial \overline{C_{IM}}}{\partial t}=\alpha(C_M-\overline{C_{IM}}) \tag{2}$$

Eqs.(1) and (2) contain two kinds of coefficients relating to mass transfer, i.e., D_x and α. The former describes the longitudinal dispersion (Taylor dispersion) in the mainstream. Previous studies indicated that the dispersion coefficient depends on the Péclet number conditions and it can be generally expressed by the following polynomial expression (Roux et al. 1998; Detwiler et al. 2000),

$$\frac{D_x}{D}=1+\alpha_{macro}Pe+\alpha_{Taylor}Pe^2 \tag{3}$$

where D is the molecular diffusion coefficient and Pe is Péclet number defined as $Pe=Ua/D$ (U: averaged flow velocity, a: channel height). α_{macro} and α_{Taylor} note the coefficients which depend on the wall roughness and the cross-sectional-shape of the channel, respectively. Under conditions of low Péclet number, the solute dispersion occurs by molecular diffusion. Thus, the dispersion coefficient is approximately the same as the molecular diffusion coefficient $D_x \sim D$ (the first term in RHS of

Eq.(3)). At moderate *Pe* conditions, the effect of wall roughness contributes to solute dispersion and the dispersion coefficient is proportional to *Pe* (the second term). The longitudinal dispersion is almost determined by the channel cross-sectional shape under conditions of large Péclet number, and the dispersion coefficient is proportional to the square of *Pe* in this case (the third term).

Moreover, the coefficient α in Eq.(2) indicates the mass transfer coefficient between mobile (mainstream) and immobile regions. This is obviously dependent on the flow condition. For example, Zhou et al. (2019) numerically investigated mass transfer from mobile to immobile regions at relatively large Reynolds number conditions. They found that the recirculation flow forms in each immobile region and the mass transfer coefficient depends on the resultant flow. At low Reynolds number flow, the coefficient α is still unknown. It is expected to be small value since the advection effect becomes insignificant in each immobile region. However, the mechanism of M-IM mass transfer at low *Re* conditions and the dependency of the mass transfer coefficient on the characteristics of wall roughness is completely unknown.

Experimental method

Figure 2 (a) presents a schematic diagram of the experimental system for quantifying the concentration field in a micro-channel. The experimental cell shown in Fig.2 (b) contains an exchangeable micro-channel and is connected to a syringe pump (Chemyx, Fusion Touch CXF1020P). The micro channel is composed of an acrylic plate and various-shaped stickers which are made of water-repellent paper with a thickness 0.2mm, shown in Fig.2 (c). The experimental cell is placed between a near-infrared (NIR) light source with a collimator lens (Hayashi, LA-100IR) and a microscope CCD camera (Trinity, IUC-130WCK2).

The details of experimental procedure can be referred in our previous study (Togi et al. 2020). Copper sulfate solution (0.42 mol/L) was introduced into the pure glycerin-filled channel with a

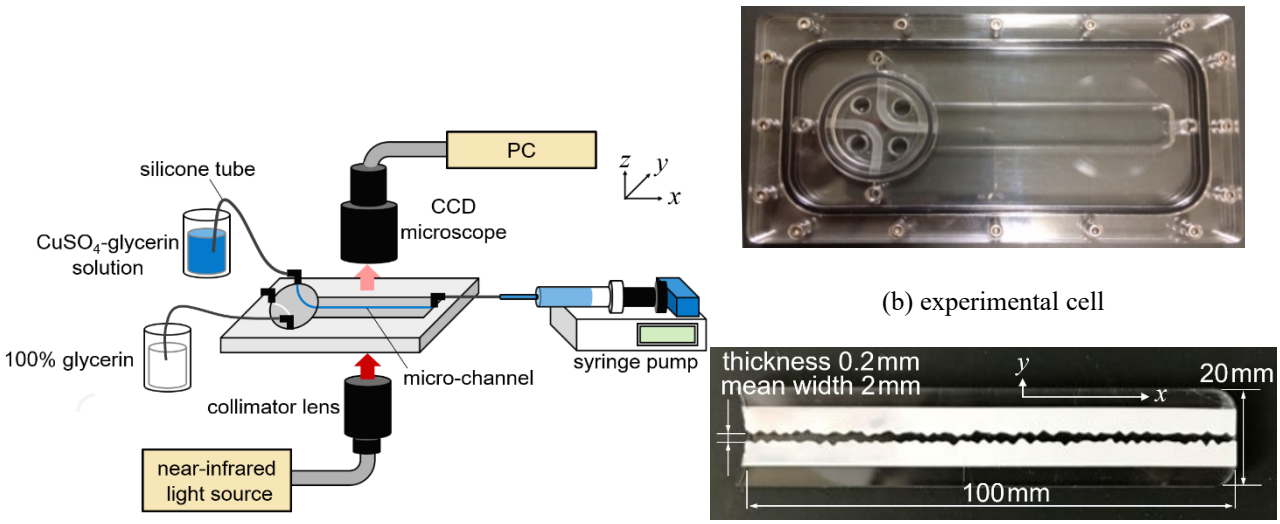

(a) experimental system

(b) experimental cell

(c) micro-channel

Fig.2 Schematic diagram of experimental system.

syringe pump with a constant volumetric flow rate Q. The reason for using glycerin was to match low Reynolds number conditions such as groundwater flow. We captured channel images with a CCD camera every 100 seconds, irradiating a parallel NIR light from the underside. Then we visualized and quantified the concentration field of cupric ions in micro-channels. Moreover, the solute concentration was quantified utilizing the absorption photometry technique based on the Lambert-Beer law. Recently, absorption photometry has been applied to visualize of a two-dimensional concentration field (Rosso et al. 1994; Otomo et al. 2014; Tanikoshi et al. 2017). As mentioned above, we used a near-infrared (NIR) light source as irradiating light in the experiment since cupric ions are likely to absorb near-NIR light with a wavelength of approximately 800 nm. We discuss mass transfer in mobile and immobile regions in the channel by quantifying the temporal change of the concentration field in the irregular-shaped micro-channel. As reported in our previous study (Togi et al. 2020), we confirmed a linear relationship between the concentration of cupric ions and the light intensity passing through a micro channel. The corresponding molar absorbance coefficient in our system is κ=17.2 $cm^{-1}M^{-1}$.

The cross-sectional dimensions of each micro-channel are given by a = 0.2 mm (height in z direction) and b = 2 mm (average width in y direction). The length of the channel in x direction is 100 mm. We designed the stickers for the rough walls with the CAD software based on Fourier sine series.

The details of the wall design is described in the previous study (Togi et al. 2020). We defined two parameters for characterizing the wall roughness of the channel, *i.e.*, the amplitude σ and the wavelength T. The amplitude σ is defined as the standard deviation of the depth of the rough-wall. The wavelength T defines the minimum wavelength of the rough wall calculated from the maximum wavenumber. The immobile regions, as described in Fig.1(b) were defined the area (volume) that extends beyond the mean width, which is shown in Fig.2(c). We varied the volumetric flow rate Q in the experiment and controlled the Péclet number $Pe=Ua/D$ ($U(=Q/ab)$: average velocity, D: molecular diffusion coefficient). The experiments were conducted under the conditions $10^2< Pe <10^3$, where the wall effect is dominant (Roux et al. 1998; Detwiler et al. 2000). In the experiment of transient dispersion shown below, the volumetric flow rate is fixed as $Q = 7\times10^{-5}$ ml/min. The corresponding Péclet number is Pe=250 and the Reynolds number is in the order of 10^{-7}.

Results and discussion

Mass transfer in mobile region

As indicated in Eq.(3), the dispersion coefficient in the mobile region (mainstream) in a rough-walled channel is complicatedly dependent on the channel geometry and flow conditions. The coefficients in Eq.(3) have been modelled using the geometric characteristics of the channel. The third term in Eq.(3) describes the effect of channel cross-section which dominates at a large Péclet number. The following model expresses the dispersion coefficient in the rectangular channel with smooth surfaces (Chatwin et al. 1982).

$$\frac{D_x}{D} = \frac{7.9512}{210}\left(1-\frac{1}{\Gamma}\right)Pe^2 \sim 0.038\left(1-\frac{1}{\Gamma}\right)Pe^2 \tag{4}$$

where $\Gamma = b/a$ is the aspect ratio of the cross-section of the rectangular channel. From Eq.(4), the coefficient should be $\alpha_{\mathrm{Taylor}} = 0.038\,(1-1/\Gamma)$.

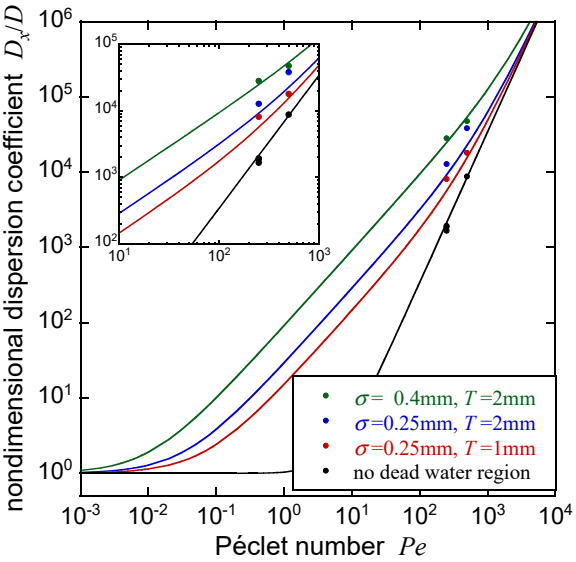

Fig. 3 Comparison of experimental and model results (reproduction of Fig.9 in Togi et al. 2020).

The second term in Eq.(3) describes the dispersion coefficient at a moderate Péclet number where the effect of wall roughness is significant. At this regime, Togi et al. (2020) modeled the dispersion coefficient in a quasi-two-dimensional channel with a roughed wall as follows.

$$\frac{D_x}{D} = \gamma \left[\frac{4\left(\frac{\sigma}{b}\right)}{1-4\left(\frac{\sigma}{b}\right)^2} \right]^2 \frac{T}{a} Pe \tag{5}$$

where σ/b is the relative amplitude of wall roughness to the channel width, T/a is the relative wavelength of wall roughness with respect to the channel thickness. Furthermore, γ is a constant and γ=10 in a quasi-two-dimensional channel. The coefficient α_{macro} in Eq.(3) can be obtained from Eq.(5).

Figure 3 shows the experimental results of the longitudinal dispersion coefficient in a quasi-two-dimensional rough-walled channel with respect to Péclet number (reproduction of Fig.9 in Togi et al. (2020)). The solid lines present the calculation results of Eq.(3) with Eqs.(4) and (5). Accordingly, the dispersion coefficients calculated by Eq.(3) sufficiently represent the experimental results for the

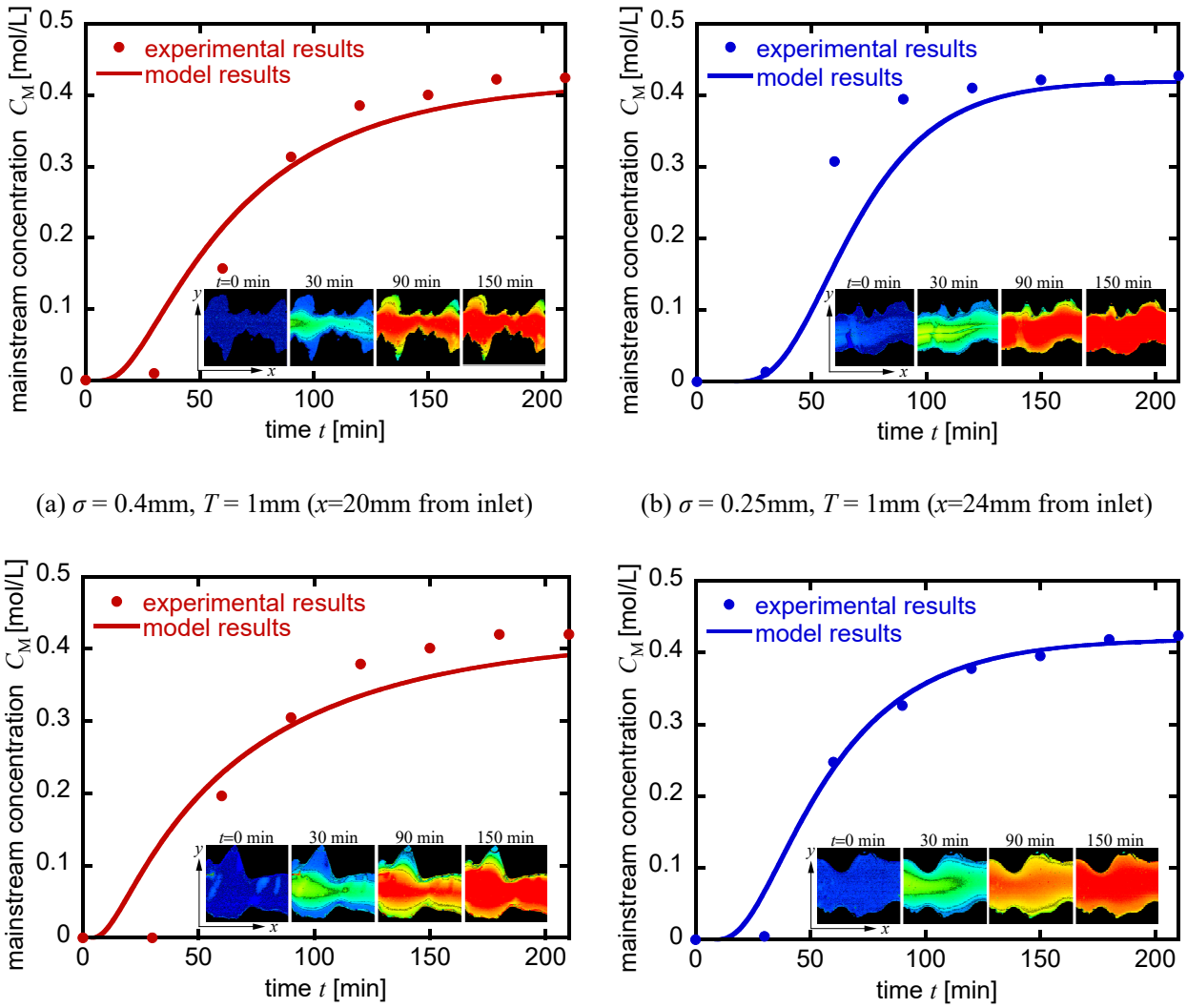

(a) σ = 0.4mm, T = 1mm (x=20mm from inlet)

(b) σ = 0.25mm, T = 1mm (x=24mm from inlet)

(c) σ = 0.4mm, T = 2mm (x=21mm from inlet)

(d) σ = 0.25mm, T = 2mm (x=17mm from inlet)

Fig. 4 Comparison of experimental and MIM model results (σ: amplitude of wall roughness, T: wavelength of wall roughness).

rough-walled channel with dead water regions. The dispersion coefficients in the channels in which the dead water region does not form coincide with the calculation results of Eq.(4). From the results shown in Fig.3, the geometric channel characteristics, especially the wall roughness and the presence of the dead water region, significantly affect the solute dispersion. The dead water region in complex-shaped flow channels has been examined in previous studies (Lee et al. 2014; Briggs et al. 2017). They reported that dead water regions formed in the channels with large amplitudes and small wavelengths of the irregularly-shaped walls.

We examined the applicability of the MIM model with the dispersion model described above to transient dispersion behavior in rough-walled channels. Figure 4 reveals the temporal change of the cross-sectional averaged concentration in the mobile region with four kinds of rough-walled channels at a specific longitudinal position from the inlet, as indicated in respective captions (center of inset pictures). The inset pictures show the quantification results of solute concentration at t = 0, 30, 90 and 150 min. around the measuring point in individual cases (red: high concentration, blue: low concentration). The inset figures show that solute transport in the mobile region greatly depends on the wall roughness. The roughness with a large amplitude and small wavelength (Fig.4a) contributes to the enhancement of streamwise dispersion in the mobile region. On the other hand, the dispersion in the channel with a small amplitude and large wavelength (Fig.4d) is similar to that in the smooth-walled channel, i.e., the parabolic concentration profile. The solid lines in Fig.4 designate the solution of the following equation combining Eq.(1) with Eqs.(4) and (5) (Chatwin et al. 1982; Togi at al. 2020);

$$(1-\sigma)\frac{\partial C_{\mathrm{M}}}{\partial t}=(1-\sigma)D\left(1+\alpha\left[\frac{4\left(\frac{\sigma}{b}\right)}{1-4\left(\frac{\sigma}{b}\right)^2}\right]^2\frac{T}{a}Pe+0.038\left(1-\frac{1}{\Gamma}\right)Pe^2\right)\frac{\partial^2 C_{\mathrm{M}}}{\partial x^2}-v\frac{\partial C_{\mathrm{M}}}{\partial x} \qquad (6)$$

where the term related to the distribution into the immobile region (the second term in LHS of Eq.(1)) was ignored because of the difference of their timescales as explained below. The ratio of the immobile region θ in Eq.(1) is replaced by the amplitude of wall roughness σ. We checked that this assumption is valid for the rough-walled channel with small wavelength (T < 2mm) by preliminary PIV experiments. We calculated the temporal change of the concentration in mobile region by numerical integration of Eq.(6), substituting the flow condition and geometric parameters of the channel.

As shown in Fig.4, the transient dispersion behavior in the mobile region can be roughly described by the model given in Eq.(6), which is composed of geometric channel characteristics. The experimental results shown in Fig.4 greatly depend on location, because the channel wall is unevenly distorted. Nevertheless, the model results almost predict the temporal change of solute concentration

in the mobile region of respective channels.

Mass transfer in immobile region

As mentioned in the previous section, the solute dispersion in the mobile region is greatly influenced by the roughness of the channel wall. We also examined the dispersion behaviors in the dead water region (immobile region). Figure 5 (a) shows the temporal change of the concentration profile in the dead water region in a rough-walled channel with an amplitude σ = 0.25mm and wavelength T =1mm. The upper figures are obtained by the quantification of the concentration field in our experiment. It should be noted that mass transfer in the immobile region occurs slowly compared to that in the mobile region. Another point to notice is that the dispersion in the immobile region almost occurs one-dimensionally from the mobile region to the edge of the immobile region. As mentioned above, Zhou et al. (2019) reported that recirculation flow plays a significant role in mass transfer in immobile regions at moderate Reynolds number conditions (Re=10~150). Alternatively, our results are obtained from the experiment under small Reynolds number conditions (Re < 1) and therefore it is in contrast to their results. The results show that there is no advection effect and pure diffusion is dominant in immobile region at low Re. This may be valid when the wall roughness has small wavelength and large amplitude like this study.

Fig.5 (b) indicates the concentration profiles obtained from a simplified numerical simulation of the following two-dimensional diffusion equation by a finite difference scheme.

$$\frac{\partial C_{IM}}{\partial t} = D\left(\frac{\partial^2 C_{IM}}{\partial x^2} + \frac{\partial^2 C_{IM}}{\partial y^2}\right) \tag{7}$$

where $C_{IM}(x, y, t)$ is the solute concentration in the immobile region and D is the molecular diffusion coefficient. We set the boundary conditions as $C_{IM} = C_0$ at $y = 0$ (i.e., the lowest line in Fig.5, or the boundary between mobile and immobile regions) and $\partial C_{IM}/\partial y = 0$ at the wall boundary of the immobile region. The molecular diffusion coefficient is set equal to that of glycerin at room temperature D=1.43 $\times 10^{-4}$ mm^2/min. and the boundary concentration is set equal to C_0=0.42mol/L.

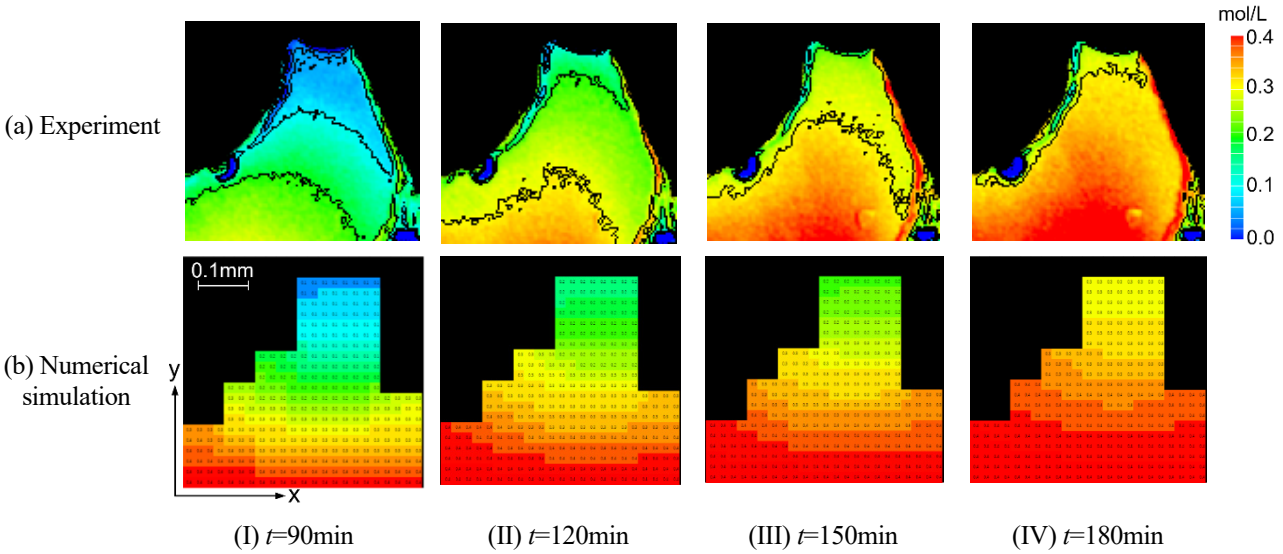

Fig. 5 Temporal change of solute concentration in immobile region. (a) quantified concentration field of immobile region in a rough-walled channel with σ= 0.25mm and T = 1mm. (b) the solution of two-dimensional diffusion equation with simplified boundary conditions. Color legends in the upper and lower figures are the same.

Although the simulation was conducted by simplifying the wall geometry as shown in Fig.5(b), the simulation results adequately describe the dispersion behavior in the immobile region observed from the experiment, particularly the timescale of mass transfer. Therefore mass transfer in the immobile region is almost governed by molecular diffusion and is unaffected by the flow under small Reynolds number conditions. Although mass transfer into the immobile region is slow compared to that in mobile region, it is not negligible as an integral value and consequently may have a significant effect on the mass transfer in mainstream, even at low Reynolds number conditions.

Mass transfer from mobile to immobile regions

As explained above, mass transfer in the immobile region occurs by molecular diffusion at small Reynolds number conditions. On the other hand, the previous studies suggest that mass transfer from mobile to immobile regions describes a kind of rate equation (first-order differential equation) given by Eq.(2) (Zhou et al. 2019). The solution of Eq.(2) is described as follows.

$$\overline{C}_{\mathrm{IM}}(t) = C_0 - Ae^{-\alpha t} \tag{8}$$

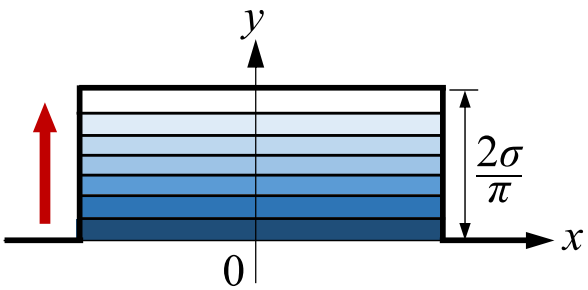

Fig. 6 Conceptional image of modeling of mass transfer in immobile region.

where $\overline{C_{IM}}$ is the averaged concentration in the immobile region, α is the mass transfer coefficient between mobile (mainstream) and immobile regions, A is an integration constant and C_0 is the inlet concentration corresponding to the concentration in the mobile region.

In order to understand the mechanism of mass transfer between M-IM regions at low *Re* conditions, we try to derive the mass transfer coefficient α analytically using a simple model and relate to geometric properties of the channel. As shown in Fig.5, mass transfer in the immobile region occurs almost one-dimensionally by molecular diffusion. Therefore we solve one-dimensional diffusion equation of the concentration in immobile region $C_{IM}(y, t)$ as follows.

$$\frac{\partial C_{IM}(y, t)}{\partial t} = D \frac{\partial^2 C_{IM}(y, t)}{\partial y^2} \tag{9}$$

where y indicates the direction perpendicular to mainstream. As shown in Fig.6, we assume an immobile region as a $T/2 \times 2\sigma/\pi$ rectangle region, which has the same area as that of a half-wavelength of a sinusoidal function $\sigma \sin(2\pi x/T)$. If mass transfer in immobile region occurs one-dimensionally, the width $T/2$ is not required. Therefore we only consider the depth of the rectangle region $2\sigma/\pi$. Considering the boundary condition $C_{IM}(0, t)=C_0$ and $\partial C_{IM}(2\sigma/\pi, t)/\partial y = 0$, Eq.(9) can be solved by Fourier series expansion as follows.

$$C_{IM}(y, t) = C_0 \left(1 - \sum_n \left(\frac{2}{\frac{\pi}{2} + n\pi} \right) e^{-D\left\{ \frac{\pi}{2\sigma}\left(\frac{\pi}{2}+n\pi\right) \right\}^2 t} \cdot \sin \frac{\pi}{2\sigma}\left(\frac{\pi}{2} + n\pi\right) y \right) \tag{10}$$

where n =0,1,2$\cdots$ is an integer. The averaged concentration in the immobile region $\overline{C}_{IM}(t)$ can be calculated by integrating Eq.(10) as follows.

$$\overline{C}_{\mathrm{IM}}(t) = \frac{\pi}{2\sigma}\int_0^{\frac{2\sigma}{\pi}} C(y,\, t)\, dy$$

$$= C_0\left(1 - \sum_n \left(\frac{2}{\left(\frac{\pi}{2} + n\pi\right)^2}\right) e^{-D\left\{\frac{\pi}{2\sigma}\left(\frac{\pi}{2}+n\pi\right)\right\}^2 t}\right) \tag{11}$$

Figure 7 presents a comparison of averaged concentration in the immobile region (dead water region) $\overline{C}_{\mathrm{IM}}$ obtained from the experiment and the solution of Eq.(11). We calculate $\overline{C}_{\mathrm{IM}}$ from the experiment by averaging the concentrations at six points in an immobile region for respective channels. While the inlet concentration (mainstream concentration) increases gradually with time in the experiment, it is assumed to be constant in the above analysis. Therefore we controlled the starting time of the analysis as only one fitting parameter. As shown in Fig.7, the analytical results of temporal

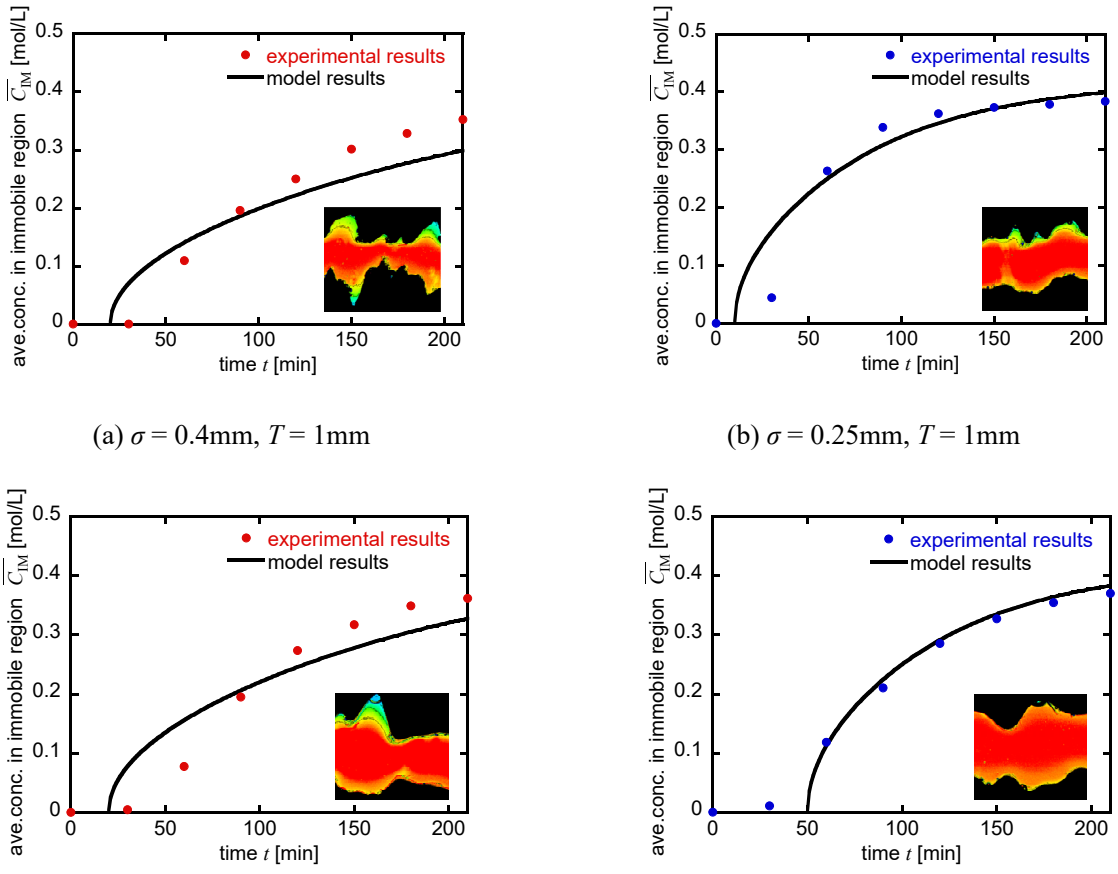

(a) σ = 0.4mm, T = 1mm

(b) σ = 0.25mm, T = 1mm

(c) σ = 0.4mm, T = 2mm

(d) σ = 0.25mm, T = 2mm

Fig. 7 Comparison of averaged concentration in immobile region obtained from experiment and analytical solution of one-dimensional diffusion equation.

change of concentration in the immobile region roughly represent the experimental results, even though our assumptions are relatively simple.

If we accept that the above assumptions are valid, i.e., mass transfer in the immobile region occursone-dimensionally by molecular diffusion under small Reynolds number conditions, we can theoretically derive the mass transfer coefficient by the following procedures. In Eq.(11), high-order terms decay rapidly with time because they include exponential functions. Substituting n=0 into Eq.(11), we obtain the approximate solution of the averaged concentration in the immobile region as follows.

$$\overline{C}_{\mathrm{IM}}(t) = C_0 - \frac{8C_0}{\pi^2} e^{-D\frac{\pi^4}{16\sigma^2}t} \tag{12}$$

Comparing Eq.(12) with Eq.(8), the mass transfer coefficient α can be instantaneously obtained as follows.

$$\alpha = D\frac{\pi^4}{16\sigma^2} \tag{13}$$

According to Eq.(13), the mass transfer coefficient α is proportional to the molecular diffusion coefficient and inversely proportional to the square of the amplitude (depth) of the immobile region. Comparing the numerical results of the original equation described in Eq.(11) and those of the simplified equation described in Eq.(12), they are indistinguishably similar, as indicated by solid lines in Fig.7. From these analyses, we can express mass transfer from mobile to immobile regions by Eq.(2) without any empirical parameters.

We emphasize that the purpose of the modeling shown here is to derive M-IM mass transfer coefficient mathematically as functions of wall roughness characteristics and understand its mechanism. We successfully extract the physical essence of mass transfer coefficient at low *Re* condition which has been completely unknown, although it is valid for a quasi-two dimensional channel.

Conclusions

We experimentally examined the laminar dispersion of solutes in channels with various irregularities of the wall surface. Mass transfer in mobile region (mainstream), immobile region (dead water region) and mobile to immobile regions were investigated under small Reynold number conditions. The concentration field in each region was visualized and quantified by absorption photometry techniques. Moreover, we developed a mass transfer model based on Mobile–Immobile concepts proposed by previous studies.

In mobile (mainstream) regions, the transient dispersion behaviors in the longitudinal direction can be expressed by an advection-dispersion equation with the dispersion coefficient for the rough-walled channel proposed by the previous studies (Togi et al., 2020). The longitudinal dispersion in the rough-walled channel was determined by the size and the cross-sectional aspect ratio of the channel, and also the geometric characteristics of the wall roughness at moderate Péclet number conditions.

In immobile (dead water) regions, the mass transfer occurs almost one-dimensionally by molecular diffusion under small Reynolds number conditions. This is in contrast to mass transfer under large Reynolds number conditions, in which the effect of circulation flow dominates mass transfer in immobile regions. Consequently, mass transfer in immobile regions was determined by the molecular diffusion coefficient independent on the geometry of wall roughness.

Mass transfer from mobile to immobile regions was determined by the concentration difference between these regions. The governing equation was the first-order differential equation with the mass transfer coefficient. A similar differential equation was also derived from one-dimensional diffusion equation of the concentration in the immobile region. By comparing these two solutions, the mass transfer coefficient was theoretically obtained as functions of molecular diffusion coefficient and the depth of wall roughness. From this result, we found a clue to the mechanism of M-IM mass transfer at low Reynolds number conditions. This is one of major achievement of this study.

From the above results, we developed a mathematical model that expresses the transient solute dispersion as functions of flow condition and geometric properties of the channel. The model reasonably predicted the transient dispersion behavior obtained from the experiment. Although the dispersion model proposed here is only applicable to the quasi-two-dimensional channels used in this study, the modeling concept can be extended for variously-shaped micro-channels.

References

Ajdari, A., N. Bontoux, and H. A. Stone. 2006. Hydrodynamic Dispersion in shallow microchannels: the effect of cross-sectional shape. *Analytical Chemistry* 78, no. 2: 387-392.

Aris, R. 1959. On the Dispersion of a solute by diffusion, convection and exchange between phases. *Proceedings of the Royal Society A, Mathematical, Physical and Engineering Sciences* 252, no. 1271: 538-550.

Bouquain, J., Y. Méheust, D. Bolster, and P. Davy. 2012. The impact of inertial effects on solute dispersion in a channel with periodically varying aperture. *Physics of Fluids* 24, no. 083602: 1-17.

Briggs. S., B. W. Karney, and B. E. Sleep. 2017. Numerical modeling of the effects of roughness on flow and eddy formation in fractures. *Journal of Rock Mechanics and Geotechnical Engineering* 9, no. 1: 105-115.

Chatwin, P. C., and J. S. Paul. 1982. The effect of aspect ratio on longitudinal diffusivity in rectangular channels. *Journal of Fluid Mechanics* 120: 347-358.

Coats, K. H., and B. D. Smith. 1964. Dead-end pore volume and dispersion in porous media. *Society of Petroleum Engineers Journal* 4: 73-84.

Detwiler, R. L., H. Rajaram, and R. J. Glass. 2000. Solute transport in variable-aperture fractures: an investigation of the relative importance of Taylor dispersion and macrodispersion. *Water Resources Research* 36, no. 7: 1611-1625.

Domenico, P. A., and F. W. Schwartz. 1998. *Physical and Chemical Hydrogeology, 2nd Edition*, Wiley & Sons, Inc.

Doshi, M. R., M. D. Pankaj, and N. G. William. 1978. Three dimensional laminar dispersion in open and closed rectangular conduits. *Chemical Engineering Science* 33, no. 7: 795-804.

Dutta, D., A. Ramachandran, A., and D. T. Leighton Jr. 2006. Effect of channel geometry on solute dispersion in pressure-driven microfluidic systems. *Microfluidics and Nanofluidics* 2: 275-290.

Fukushima, K., and N. Hayakawa. 1983. Laminar dispersion in an elliptical pipe and in a rectangular pipe. *Journal of Japan Society of Fluid Mechanics* 2: 34-42.

Gao, G., H. Zhan, S. Feng, B. Fu, Y. Ma, and G. Huang. 2010. A new mobile-immobile model foe reactive solute transport with scale-dependent dispersion, *Water Resources Research* 46: W08533.

Haggerty, R., and S. M. Gorelick. 1995. Multiple-rate mass transfer for modeling diffusion and surface reactions in media with pore-scale heterogeneity. *Water Resources Research* 31, no.10: 2383-2400.

Jury, W. A., and R. Horton. 2004. *Soil Physics, 6th Edition*, Wiley & Sons, Inc.

Koplik, J., I. Ippolito, and J. P. Hulin. 1993. Tracer dispersion in rough channels: a two dimensional numerical study. *Physics of Fluids A* 5: 1333-1343.

Lee, S. H., K.-K. Lee, and I. W. Yeo. 2014. Assessment of the validity of Stokes and Reynolds equations for fluid flow through a rough-walled fracture with flow imaging. *Geophysical Research Letters* 41, no.13: 4578-4585.

Otomo, R., N. Ishii, K. Takahashi, and S. Harada. 2014. Mass transfer caused by gravitational instability at reactive solid-liquid interfaces. *Journal of Visualization* 17, no. 1: 49-57.

Porta, G., S. Chaynikov, M. Riva, and A. Guadagnini. 2013. Upscaling solute transport in porous media from the pore scale to dual- and multicontinuum formulations. *Water Resources Research* 49: 2025-2039.

Rosso, M., J. N. Chazalviel, and V. Fleury, and E. Chassaing. 1994. Experimental evidence for gravity induced motion in the vicinity of ramified electrodeposits. *Electrochimica Acta* 39, no. 4: 507-515.

Roux, S., F. Plouraboué, and J. P. Hulin. 1998. Tracer dispersion in rough open cracks. *Transport in Porous Media* 32: 97-116.

Tanikoshi, T., R. Otomo, and S. Harada. 2017. Quantitative evaluation of mass transfer near the edge of porous media by absorption photometry. *AIChE Journal* 63, no. 2: 823-833.

Taylor, G. 1953. Dispersion of soluble matter in solvent flowing slowly through a tube. *Proceedings of the Royal Society A, Mathematical, Physical and Engineering Sciences* 219, no.1137: 186-203.

Togi, F., T. Kubota, K. Toyama, A. Ishida, and S. Harada. 2020. Quantitative evaluation of solute dispersion in irregularly shaped micro-channels. *Microfluidics and Nanofluidics* 24, no.57: 1-8.

Stone, H. A., A. D. Stroock, and A. Ajdari. 2004. Engineering flows in small devices: microfluidics toward a lab-on-a-chip. *Annual Review of Fluid Mechanics* 36: 381-411.

van Genuchten, M. T., and P. J. Wierenga. 1976. Mass transfer studies in sorbing porous media I. analytical solutions. *Soil Science Society of America Journal* 40: 473-480.

Wang, L., M. B. Cardenas, J.-Q. Zhou, and R. A. Ketcham. 2020. The complexity of nonlinear flow and non-Fickian transport in fractures driven by three-dimensional recirculation zones. *Journal of Geophysical Research: Solid Earth* 125, no.9: e2020JB020028.

Yoon, S., and P. K. Kang. 2021. Roughness, inertia, and diffusion effects on anomalous transport in rough channel flows. *Physical Review Fluids* 6: 014502.

Zhou, J.-Q., L. Wang, Y.-F. Chen, and M. B. Cardenas. 2019. Mass transfer between recirculation and main flow zones: Is physically based parameterization possible? *Water Resources Research* 55: WR023124.

List of Figures